Phase reduction technique on a target region

Makoto Iima*

Graduate School of Integrated Life Sciences, Hiroshima University, 1-7-1, Kagamiyama Higashihiroshima, Hiroshima 739-8521, Japan

(Received 31 January 2021; accepted 15 April 2021; published 10 May 2021)

We propose a phase reduction technique that provides the phase sensitivity function, which is one of the essential functions in phase reduction theory, on a target region. A system with a large degree of freedom and global coupling, such as an incompressible fluid system, is emphasized. Such a system poses challenges for the numerical calculation of the phase sensitivity function, which cannot be resolved using known algorithms such as the direct method or the adjoint method. A combination of the Jacobian-free algorithm and the Rayleigh-Ritz procedure is proposed to significantly reduce the computational cost and obtain a good approximation of the phase sensitivity function in a particular region of interest. In addition, the approximation can be assessed using the Ritz value. The breathing solution of a reaction-diffusion system and the flow past a flat plate are used to analyze the proposed methods, and the characteristics of the proposed method are discussed.

DOI: 10.1103/PhysRevE.103.053303

I. INTRODUCTION

Phase reduction theory has been applied to rhythmic phenomena in a wide range of research fields, such as engineering (mechanical vibrations), chemistry (Brillouin-zone reactions), ecology (flashing fireflies), and physiology (circadian rhythms); it provides a simple and clear vision of the essential part of the dynamics. In terms of dynamical systems, phase reduction theory can be used to analyze the state near a limit cycle (LC). The state near an LC can be described by a single variable "phase," ϕ, and the dynamics of the phase describes the response to the perturbation, entrainment to the external oscillating force, and synchronization among oscillating objects (oscillators) [1,2].

In many rhythmic phenomena, phase synchronization or phase entrainment is suggested, although a detailed mathematical analysis using phase reduction theory has been applied to limited cases in which simple model equations are provided. Even if a mathematical model is available, the application of phase reduction theory is not always straightforward because of the computational cost; a typical example is the incompressible fluid system.

An essential function of the phase reduction theory is the phase sensitivity function, which describes the phase shift between two states in close proximity and is used for analyzing perturbed systems or synchronization among oscillators. To calculate the phase sensitivity function, two methods are used [2]: the direct method, in which the phase shift between a perturbed and an unperturbed system is directly evaluated by the long-term evolution of those states until convergence; and the adjoint method [3], in which the adjoint equation of the original system is integrated into the inverse time direction until convergence, where the Jacobian along all the points in the LC is required.

Although the adjoint method has been widely used to analyze many rhythmic phenomena, a computational limitation may apply when the explicit form of the Jacobian is not available. A typical case is a spatiotemporal phenomenon with different time scales; when fast phenomena are included to slow phenomena as a (quasi-)steady state, the state is obtained by solving a partial differential equation (PDE), such as the Poisson equation (e.g., pressure in a fluid system or assembled cells, and thermal or concentration distributions) or the Helmholtz equation (e.g., standing waves inside structures or organs). In such cases, it is difficult to apply the adjoint method because such PDEs must be solved to calculate the Jacobian and the data must be stored for calculation; this requires a significant amount of memory particularly when the number of degrees of freedom of the system is large. For an incompressible fluid, the Poisson equation must be solved to determine the pressure. Therefore, phase reduction theory has been applied to limited cases using the direct method [4–7]; otherwise, the Hele-Shaw flow [8], or Stokes flow, which do not require the solution of the Poisson equation, is used. Recently, Kawamura successfully calculated the phase sensitivity function of the traveling wave of an incompressible fluid system with solid boundaries [9]. He derived an algebraic PDE as an adjoint system and included the solid boundary condition. However, the boundary conditions for an adjoint system are generally complicated [10]. The implementation of various boundary conditions used in more practical systems remains challenging, and efficient and convenient methods are desired.

Recently, Iima proposed a Jacobian-free algorithm to resolve these problems [11]. This method can reduce the computational cost compared with known methods, and the entire algorithm can be constructed without an adjoint system; only the time evolution algorithm of the system is required. The proposed method was used to analyze von Kármán's vortex street [12] to determine the spatial distribution of the phase sensitivity function [11,13].

*iima@hiroshima-u.ac.jp

However, for more practical problems with large degrees of freedom, further reductions are required. In particular, the demand to obtain the phase sensitivity function on only a target region is critical because we are often interested in information in a limited region instead of in the entire computational domain, which is typically set sufficiently large to reduce the effects of the domain boundary.

Herein, we propose a technique for calculating the phase sensitivity function. This technique, which is used in combination with the Jacobian-free method [11], further reduces the computational cost by focusing on the target region during analysis. Moreover, this technique can be applied to problems in which the known methods cannot be analyzed owing to the complexity of the system.

The remainder of this paper is organized as follows. In Sec. II, the theoretical background of the proposed method is discussed based on summarizing the method in Ref. [11]. In Sec. III, the property of the proposed method is discussed based on an application to a reaction-diffusion system and incompressible fluid system. In Sec. IV, the results are summarized.

II. THEORY

A. The Jacobian-free algorithm for calculation of the phase sensitivity function

We provide a short summary of the definitions and notations of the phase reduction theory and Jacobian-free algorithm to calculate the phase sensitivity function, which will be combined with the method proposed herein. Studies that involve the phase reduction theory abound, including Refs. [1,2]. For the Jacobian-free algorithm, Ref. [11] provides more detailed information.

Let us consider the n-dimensional autonomous dynamical systems expressed as

$$\frac{d\boldsymbol{x}}{dt} = \boldsymbol{f}(\boldsymbol{x}), \tag{1}$$

where $\boldsymbol{x} = {}^t(x_1, \cdots, x_n) \in \mathbb{R}^n$ and $\boldsymbol{f}(\boldsymbol{x}) = {}^t(f_1(\boldsymbol{x}), \cdots, f_n(\boldsymbol{x})) : \mathbb{R}^n \mapsto \mathbb{R}^n$, respectively. It is assumed that Eq. (1) has a stable LC solution $\boldsymbol{x}(t) = \boldsymbol{p}(t)$, where $\boldsymbol{p}(t+T) = \boldsymbol{p}(t)$ for all t, and T is the natural period.

In the phase reduction theory, the (asymptotic) phase ϕ of the state $\boldsymbol{x}$ is defined as follows [2]: The phase of the state on the LC is defined by the time measured from the origin: $\phi(t) = \omega t \pmod{2\pi}$, where $\omega = 2\pi/T$. We denote the solution to Eq. (1) with $\boldsymbol{x}(0) = \boldsymbol{x}_0$ by $\boldsymbol{x}(t;\boldsymbol{x}_0)$. Subsequently, the phase of the state $\boldsymbol{x}_0$ near the LC, $\Phi(\boldsymbol{x}_0)$, is defined by $\Phi(\boldsymbol{x}_0) = \phi_0$, where ϕ_0 is determined using the equation $\lim_{t\to\infty}[\boldsymbol{x}(t;\boldsymbol{x}_0) - \boldsymbol{p}(t+\phi_0/\omega)] = 0$. Hence, the phase variable $\Phi(\boldsymbol{x}) \in [0, 2\pi)$ is defined near the LC, in which the phase of the perturbed state can be discussed based on the LC. By introducing the phase variable ϕ, Eq. (1) is reduced to the phase equation, $d\phi/dt = \omega$.

An essential function of the phase reduction theory is the phase sensitivity function, $\boldsymbol{Z}(\phi)$. This function describes the phase shift between two near-LC states in close proximity, $\Delta\Phi$, in the following form:

$$\Delta\Phi = \Phi(\boldsymbol{x}+\Delta\boldsymbol{x}) - \Phi(\boldsymbol{x}) = \boldsymbol{Z}(\phi)\cdot\Delta\boldsymbol{x} + O(|\Delta\boldsymbol{x}|^2), \tag{2}$$

where $\boldsymbol{Z}(\phi)$ is defined as follows:

$$\boldsymbol{Z}(\phi) = \left.\frac{\partial\Phi(\boldsymbol{x})}{\partial\boldsymbol{x}}\right|_{\Phi(\boldsymbol{x})=\phi}. \tag{3}$$

The phase sensitivity function is used to calculate the phase equation of the perturbed system in Eq. (1); if we consider the perturbed equation $d\boldsymbol{x}/dt = \boldsymbol{f}(\boldsymbol{x}) + \epsilon\boldsymbol{g}(t,\boldsymbol{x})$, where ϵ is a small parameter, then the phase equation now becomes $d\phi/dt = \omega + \epsilon\boldsymbol{Z}(\phi)\cdot\boldsymbol{g}(t, \boldsymbol{p}(\phi/\omega))$. These applications are discussed in Refs. [1,2].

In the adjoint method, $\boldsymbol{Z}(\phi)$ is obtained using the periodic solution of the following adjoint equation:

$$\frac{d\tilde{\boldsymbol{Z}}}{dt} = -{}^tJ[\boldsymbol{p}(t)]\tilde{\boldsymbol{Z}}, \tag{4}$$

where J is the Jacobian matrix of the dynamical system (1); its (i,j) component J_{ij} is $J_{ij} = \partial f_i/\partial x_j$ [3], and $\tilde{\boldsymbol{Z}}(t) = (1/\omega)\boldsymbol{Z}(\omega t)$ under normalization $\tilde{\boldsymbol{Z}}(t)\cdot\boldsymbol{f}[\boldsymbol{p}(t)] = 1$.

It can be shown that $\boldsymbol{Z}(\phi)$ is proportional to the vector function $\boldsymbol{z}_p(t) \in \mathbb{R}^n$ that satisfies

$${}^t\boldsymbol{z}_p(t)[G_p(t+T) - G_p(t)] = 0, \tag{5}$$

where $n\times n$ matrix $G_p(t)$ is the fundamental solution matrix of the following linear equation of $\boldsymbol{y}$:

$$\frac{d\boldsymbol{y}}{dt} = J[\boldsymbol{p}(t)]\boldsymbol{y}. \tag{6}$$

Equation (5) can be derived through both the adjoint equation [11] and the direct method [14].

Iima [11] proposed an efficient method for calculating $\boldsymbol{Z}(\phi)$ as follows. It is noteworthy that $G_p(t)$ can be estimated without differentiation using the following formula,

$$\begin{aligned}&\boldsymbol{x}(t_0+T;\boldsymbol{p}(t_0)+\boldsymbol{y}_0) - \boldsymbol{x}(t_0;\boldsymbol{p}(t_0)+\boldsymbol{y}_0)\\ &\simeq [G_p(t_0+T) - G_p(t_0)]\boldsymbol{y}_0,\end{aligned} \tag{7}$$

for small $\boldsymbol{y}_0$. Using Eq. (7), we can obtain the column vectors of $G_p(t+T) - G_p(t)$, whereby $\boldsymbol{z}_p(t)$ can be constructed by applying the Gram-Schmidt orthogonalization.

As shown above, this method does not require an explicit expression of the Jacobian; therefore, memory is not required to store the Jacobian data over one period. In addition, this method requires only a one-period time evolution per one column vector of $G_p(t+T) - G_p(t)$ and does not require time evolution calculations until convergence; hence, computation time is reduced compared with the direct method. However, we require the periodic solution data $\boldsymbol{p}(t)$ before calculating $\boldsymbol{z}_p(t)$, which can be obtained by using the Newton-Raphson method [15]. Further discussions regarding the characteristics of this method and a comparison with other methods are available in Refs. [11,14].

B. Redundancy and efficiency

Under some practical problems, the calculation algorithm may be modified because all of the degrees of freedom are not always significant for the major part of the phase sensitivity function. We discuss the typical cases below.

The first case is related to a large computational domain. Many PDE problems, including incompressible fluids, correspond to this case. In this case, a large computational domain

must be prepared such that the domain boundary will not affect the quantities of interest, such as the lift or drag coefficients. However, the response to the perturbation at a point far from the region of interest will be small and may not be significant. Therefore, a method that focuses on such a target region will be highly beneficial.

The second case occurs when the variables are not independent, e.g., a two-dimensional incompressible fluid. The incompressible Navier-Stokes equations contain three variables, u, v, and p, which are the x and y components of velocity and pressure, respectively. The variables u and v are not independent because they satisfy the continuity equation $\partial u/\partial x + \partial v/\partial y = 0$. In addition, p can be calculated using the Poisson equation based on the source term determined using u and v alone. In some cases, these variables can be reduced by introducing other variables such as the stream functions [16]. However, when applying the phase reduction theory to practical problems, the phase response to the perturbation to controllable variables must be determined, e.g., velocities and pressure. Therefore, variable reduction may not be the ultimate solution in all cases, despite the apparent increase in the number of degrees of freedom to compensate for the computational cost.

The third case involves the time-integration algorithm. In some multistep algorithms, we use the step information at one or more steps prior to the current time step to evaluate the future state. In such a case, the number of degrees of freedom in the discretized system is enhanced. A comprehensive case is the time discretization by the Adams-Bashforth method, which discretizes Eq. (1) as

$$\boldsymbol{x}_{k+1} = \boldsymbol{x}_k + \tfrac{3}{2}h\boldsymbol{f}(\boldsymbol{x}_k) - \tfrac{1}{2}h\boldsymbol{f}(\boldsymbol{x}_{k-1}), \tag{8}$$

where $\boldsymbol{x}_k = \boldsymbol{x}(kh)$ and h is the time step. This algorithm is a map from $(\boldsymbol{x}_k, \boldsymbol{x}_{k-1})$ to $(\boldsymbol{x}_{k+1}, \boldsymbol{x}_k)$ and $2n$ degrees of freedom are required to describe the time evolution by the algorithm. In fact, we must solve the $2n$ dynamical system to obtain the periodic solution using the Newton-Raphson method using this algorithm.

In summary, the target region is not intended for only the spatial region of interest, but also for the information of interest for the system. In the next subsection, we propose a method.

C. Proposed algorithm: Projection method

In this section, we propose an algorithm that approximates the solution of Eq. (5). We begin with the transposition of Eq. (5):

$$A\boldsymbol{z}_p(t) = \boldsymbol{0},\ A = {}^t[G_p(t+T) - G_p(t)] \in \mathbb{R}^{n\times n}, \tag{9}$$

which is regarded as a zero-eigenvalue problem herein.

The Rayleigh-Ritz procedure [17] can be applied to an approximate subspace of the invariant subspace F of the linear mapping determined using A. Suppose that the eigenvector $\boldsymbol{z}$ of A associated with the eigenvalue λ, i.e., $A\boldsymbol{z} = \lambda\boldsymbol{z}$, satisfies $\boldsymbol{z} \in F$. Let $m = \dim F$ and the orthonormal basis of F be $\boldsymbol{v}_1, \cdots, \boldsymbol{v}_m$ $(m \leqslant n)$ for defining the $n \times m$ matrix $V = [\boldsymbol{v}_1, \cdots, \boldsymbol{v}_m]$. Subsequently, $\boldsymbol{z}$ is represented as $\boldsymbol{z} = V\boldsymbol{y}$ $(\boldsymbol{y} \in \mathbb{R}^m)$; therefore,

$$B\boldsymbol{y} = \lambda\boldsymbol{y}, \quad B = {}^tVAV \in \mathbb{R}^{m\times m}. \tag{10}$$

In this case, we can obtain the eigenvalue and eigenvectors of the matrix A by solving an eigenvalue problem using the $m \times m$ matrix B, which is of a smaller size. In practical applications, we prepare a subspace F', which is an approximate of F. Subsequently, a similar relationship $\boldsymbol{z} = V'\boldsymbol{y}'$, where $V' = [\boldsymbol{v}'_1, \cdots, \boldsymbol{v}'_{m'}]$ $(m' = \dim F)$ is an $n \times m'$ matrix and $\boldsymbol{v}'_1, \cdots, \boldsymbol{v}'_{m'}$ is the orthonormal basis of F', is established to provide an approximation of F. Therefore, the corresponding equation is

$$B'\boldsymbol{y}' = \lambda'\boldsymbol{y}', \quad B' = {}^tV'AV' \in \mathbb{R}^{m'\times m'}, \tag{11}$$

which is expected to provide a good approximation of the set of the eigenvalues and the eigenvectors of the original eigenvalue problem. Such a reduction technique, i.e., the Rayleigh-Ritz procedure [17], has been applied to many problems involving large degrees of freedom. The approximated eigenvalue λ' is referred to as "Ritz value" hereafter.

For the current problem, we must calculate the eigenvector associated with the zero eigenvalue of A. However, the corresponding eigenvalue of B' may not be exactly zero because F' is not identical to F and because of numerical errors. Therefore, we assume that B' has a small absolute eigenvalue but is invertible to solve Eq. (11) for the absolute minimum eigenvalue, $\lambda_{\min}$, instead of the zero-eigenvalue problem. Furthermore, we regarded the corresponding eigenvector $\boldsymbol{y}'_{\min}$ as an approximation of the eigenvector of the original problem.

To calculate $\boldsymbol{y}'_{\min}$, the inverse power method can be used. Consider a sequence $\boldsymbol{y}_0, \boldsymbol{y}_1, \cdots$ determined using

$$\boldsymbol{y}_{k+1} = B'^{-1}\boldsymbol{x}_k,\ \boldsymbol{x}_k = \frac{\boldsymbol{y}_k}{|\boldsymbol{y}_k|}. \tag{12}$$

For almost any $\boldsymbol{y}_0$, the sequence converges rapidly to $\boldsymbol{y}'_{\min}$ if $|\lambda_{\min}|$ is sufficiently small [17]. If λ_1 is the eigenvalue of B', the absolute value of which is next closest to zero, then the convergence factor is expressed as $|\lambda_{\min}|/|\lambda_1|$, which is expected to be small if F' approximates F well.

It is noteworthy that the value of $\lambda_{\min}$ reflects the proximity of F' to F, i.e., it is equivalent to a relative residue of the original eigenvalue problem, $A\boldsymbol{z} = \lambda\boldsymbol{z}$ where $\lambda = 0$. In fact, the residue $\boldsymbol{r} = A\boldsymbol{z}' - \lambda\boldsymbol{z}' = A\boldsymbol{z}'$ satisfies

$$\frac{|\boldsymbol{r}|}{|\boldsymbol{z}'|} = |\lambda_{\min}|, \tag{13}$$

where $\boldsymbol{z}' = V'\boldsymbol{y}'_{\min}$. Hence, the value of $|\lambda_{\min}|$ is a measure of the validity of the solution $\boldsymbol{z}'$.

Once $\boldsymbol{y}'_{\min}$ is obtained, the eigenvector, $\boldsymbol{x}'_{\min}$, is expressed as $\boldsymbol{x}'_{\min} = V'\boldsymbol{y}'_{\min}$, and the phase sensitivity function is estimated by the procedure detailed in Sec. II A of Ref. [11]. Hereinafter, the proposed method is known as "the projection method," and the estimated phase sensitivity function is known as the "projected phase sensitivity function."

D. Phase sensitivity function for the reduced system

In this section, we estimate the error of the projected phase sensitivity function. We consider a dynamic system expressed as

$$\frac{d\boldsymbol{u}}{dt} = \boldsymbol{f}(\boldsymbol{u}), \tag{14}$$

which is the same as that in Eq. (1) but the variables are changed to $\boldsymbol{u}$, as a spatially discretized system of a PDE. For simplicity, we consider the one-dimensional PDE of a single component $u(x,t)$ in the domain $(x,t) \in [0,L] \times [0,\infty]$ (L is the spatial length scale):

$$\frac{\partial u}{\partial t} = \mathcal{F}(\{u(x,t)\}), \tag{15}$$

where $\mathcal{F}$ is a function of u. It is assumed that Eq. (15) has an LC and the state near the LC is considered.

Let us discretize the space by n grid points, e.g., $u_k(t) = u(x_k,t)$, where $x_k = (k-1/2)\Delta x$ and $\Delta x = L/n$ ($k = 1, 2, \cdots, n$) to define $\boldsymbol{u} = (u_1, \cdots, u_n)$.

When n is changed, $G_p(t)$ is scaled as $1/n$ for the following reason. First, we denote the dimension of u, as well as each element of $\boldsymbol{u}$, as $[\mathsf{U}]$. The dimension of $\mathcal{F}$ is $[\mathsf{U}\mathsf{T}^{-1}]$, where T is the time unit. Subsequently, the Jacobian of $\mathcal{F}$, J, has the dimension $[\mathsf{U}\mathsf{T}^{-1}\mathsf{L}^{-1}]$, where L is the spatial length unit. Under the change in n, the components of $\boldsymbol{u}$ are invariant, but the components of J are scaled as $1/n$ because the magnitude of the right-hand side of the linearized equation (6) does not depend on n when n is large. Hence, $G_p(t)$ is also scaled to $1/n$.

For the following analysis, the phase space ($\mathbb{R}^n$) is segmented into two subspaces, W_1 and W_2, both of which are the linear spaces. Here, W_1 ($\dim W_1 = m$) corresponds to the target region where the phase sensitivity function assumes significant values, and $W_2 = \mathbb{R}^n \setminus W_1$ is the region outside the target region where the magnitude of the phase sensitivity function is not significant.

Further, we assume that $\mathbb{R}^n$ is represented by the direct sum of W_1 and W_2: $\mathbb{R}^n = W_1 \bigoplus W_2$, where $W_1 = \mathrm{span}\{\boldsymbol{v}_1, \cdots, \boldsymbol{v}_m\}$ and $W_2 = \mathrm{span}\{\boldsymbol{v}_{m+1}, \cdots, \boldsymbol{v}_n\}$, where $\boldsymbol{v}_1, \cdots, \boldsymbol{v}_m$ and $\boldsymbol{v}_{m+1}, \cdots, \boldsymbol{v}_n$ are the orthonormal bases of W_1 and W_2, respectively. We define the matrices, $V_1 = [\boldsymbol{v}_1, \cdots, \boldsymbol{v}_m]$ ($\in \mathbb{R}^{n\times m}$), $V_2 = [\boldsymbol{v}_{m+1}, \cdots, \boldsymbol{v}_n]$ ($\in \mathbb{R}^{n\times(n-m)}$), and $V = [\boldsymbol{v}_1, \cdots, \boldsymbol{v}_n] = [V_1 \quad V_2] (\in \mathbb{R}^{n\times n})$, which is an orthonormal matrix.

Next, the matrix representation of the linear mapping by $G_p(T)$ in the base $\boldsymbol{v}_1, \cdots, \boldsymbol{v}_n$, M, is expressed as

$$G_p(T)V = [\boldsymbol{v}_1', \cdots, \boldsymbol{v}_n'] = VM, \tag{16}$$

$$M = \left[\begin{array}{c|c} M_{11} & m_{12} \\ \hline m_{21} & m_{22} \end{array}\right], \tag{17}$$

where M_{11}, m_{12}, m_{21}, and m_{22} are the $m\times m, m\times(n-m), (n-m)\times m$, and $(n-m)\times(n-m)$ matrices, respectively.

The assumption above results in the magnitude of the components of these matrices, as follows: A small parameter ϵ is introduced to evaluate the dependency of the magnitude on n and ϵ. We assume that the components of M_{11} are scaled by $O(1)/n$, whereas the components of m_{12}, m_{21}, and m_{22} are scaled by $O(\epsilon)/n$. These assumptions imply that the linear mapping $G_p(T)$ is significant within W_1 alone.

By multiplying ${}^t\tilde{\boldsymbol{z}}$ from the left side of Eq. (16), we obtain

$${}^t\tilde{\boldsymbol{z}}V = {}^t\tilde{\boldsymbol{z}}VM, \tag{18}$$

because ${}^t\tilde{\boldsymbol{z}}G_p(T) = {}^t\tilde{\boldsymbol{z}}$ using Eq. (5). Subsequently, ${}^t\tilde{\boldsymbol{z}}V$ is decomposed as

$${}^t\tilde{\boldsymbol{z}}V = [{}^t\tilde{\boldsymbol{z}}V_1, {}^t\tilde{\boldsymbol{z}}V_2] = [{}^t\boldsymbol{z}_1, {}^t\boldsymbol{z}_2], \tag{19}$$

where $\boldsymbol{z}_1$ and $\boldsymbol{z}_2$, which are the m- and $(n-m)$-dimensional vectors, respectively, are introduced.

Equation (18) is now rewritten as

$${}^t\boldsymbol{z}_1 = {}^t\boldsymbol{z}_1 M_{11} + {}^t\boldsymbol{z}_2 m_{21}, \tag{20}$$

$${}^t\boldsymbol{z}_2 = {}^t\boldsymbol{z}_1 m_{12} + {}^t\boldsymbol{z}_2 m_{22}. \tag{21}$$

Let us assume that the components of $\boldsymbol{z}_1$ and $\boldsymbol{z}_2$ are assumed to be $O(1)$ and $O(\epsilon^a)$ (a is a non-negative integer), respectively. Subsequently, the order-balance equation derived from Eq. (21) is

$$O(\epsilon^a) = \frac{m}{n}O(\epsilon) + \frac{n-m}{n}O(\epsilon^{a+1}). \tag{22}$$

When $m/n = O(\epsilon^b)$, we obtain $a = b+1$ and $\boldsymbol{z}_2 = O(\epsilon^{b+1})$. Therefore, the second term on the right-hand side of Eq. (20) is $O(\epsilon^{b+2})$:

$${}^t\boldsymbol{z}_1 = {}^t\boldsymbol{z}_1 M_{11} + O(\epsilon^{b+2}). \tag{23}$$

Based on this analysis, we applied perturbation analysis to Eq. (23). We divide ${}^t\boldsymbol{z}_1$ into two parts as

$${}^t\boldsymbol{z}_1 = {}^t\bar{\boldsymbol{z}}_1 + {}^t\boldsymbol{z}_1', \tag{24}$$

where ${}^t\bar{\boldsymbol{z}}_1$ is the eigenvector associated with the absolute minimum eigenvalue of $M_{11} - I_m$, i.e.,

$${}^t\bar{\boldsymbol{z}}_1(M_{11} - I_m) = \lambda_{\min}{}^t\bar{\boldsymbol{z}}_1. \tag{25}$$

Subsequently, ${}^t\boldsymbol{z}_1' = O(\max(\epsilon^{b+2}, |\lambda_{\min}|)$. Equation (25) is equivalent to Eq. (11) when W_1 is selected as F'. This analysis suggests that the error of ${}^t\boldsymbol{z}_1, \boldsymbol{z}_1'$, is $O(\epsilon^{b+2})$ if $\lambda_{\min}$ is smaller than $O(\epsilon^{b+2})$ terms, whereas the components of the omitted part of the matrix M are $O(\epsilon)$; in this regard, the phase sensitivity function in a target region yielded by the projection method approximates the original phase sensitivity function well in this sense.

In summary, the projection method is equivalent to omitting the $O(\epsilon^{b+2})$ terms in Eq. (23) if $\lambda_{\min}$ is sufficiently small and to approximating the solution $\boldsymbol{z}$ as ${}^t[{}^t\boldsymbol{z}_1, \boldsymbol{0}]$. Because $b \geqslant 0$, the omitted terms are $O(\epsilon^2)$ or smaller. The ratio m/n corresponds approximately to the ratio of the target region to the entire computational domain if all the computational grid distances are equal. Typically, the entire computational domain is designed to be sufficiently large such that the effect of the domain boundary is damped. In this case, the response to the perturbation is expected to be small near the boundary. In the next section, we demonstrate the projection method using the oscillatory motion of the spatially localized solution (breathing solution) and the flow past the flat plate.

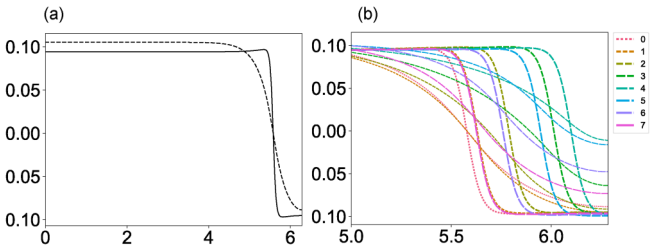

FIG. 1. (a) Snapshot of (w, v) for phase zero in the entire domain. Variables w and v are represented by the solid line and broken lines, respectively. (b) Eight snapshots obtained from solutions during one cycle in the domain $[5.0, L]$.

III. NUMERICAL EXAMPLES

A. Analysis of the breathing solution of a reaction-diffusion system

1. Breathing solution

In this subsection, we validate the projection method by analyzing the breathing solution of a one-dimensional, two-component, reaction-diffusion system [18–20]. This solution contains an interface, which is the region where the variable changes rapidly and oscillates within a confined region.

The governing equations are as follows:

$$\epsilon\tau\frac{\partial u}{\partial t} = F(u,v) + \epsilon^2\frac{\partial^2 u}{\partial x^2}, \tag{26}$$

$$\frac{\partial v}{\partial t} = G(u,v) + \frac{\partial^2 v}{\partial x^2}, \tag{27}$$

$$F(u,v) = u(1-u^2) - v, \quad G(u,v) = u + d - 8v, \tag{28}$$

where $u(x,t)$ and $v(x,t)$ are independent variables of x and t, respectively, and ϵ, τ, and d are the constants. For the practical application, we change the variable $u(x,t)$ to $w(x,t) = ku(x,t)$, where k is a constant, to set the orders of two independent variables and the phase sensitivity functions to be the same. Hereinafter $w(x,t)$ and $v(x,t)$ will be used as the independent variables. This change in the variables is important for discussing the phase sensitivity function outside the target region. We remark that the change in variables does not change to the system described by Eqs. (26)–(28).

The computational domain is $[0, L]$, and the Neumann boundary condition is applied at both ends of the domain: $\partial u/\partial x = \partial v/\partial x = 0$ at $x = 0, L$. The parameters were set as $\epsilon = 0.05$, $\tau = 0.04$, $d = -0.1$ following Ref. [21], and we set $L = 2\pi$ and $k = 10$. The computational domain was divided by N equal widths where $N = 400$. The time evolution was performed by the fourth order Runge-Kutta method.

The periodic solutions of Eqs. (26)–(28), known as "the breathing solution" [21], are obtained via the Newton-Raphson method for the periodic solution [11,15]. The relative error of the residue to the amplitude was less than 10^{-12}. The natural period of the breathing solution, T, was $T = 1.073\,300$ when one period was segmented into 20 000 equal time steps.

Figure 1 shows a snapshot of the breathing solution at a timing where the zero-crossing point of w is minimum, which is defined as the origin of the phase (phase zero). In Fig. 1(a), fields of (w, v) are shown in the entire domain. The significant value change only occurs within a confined region to the left. Owing to the change in variables, the orders of magnitudes of w and v are the same, implying that the magnitude of u is

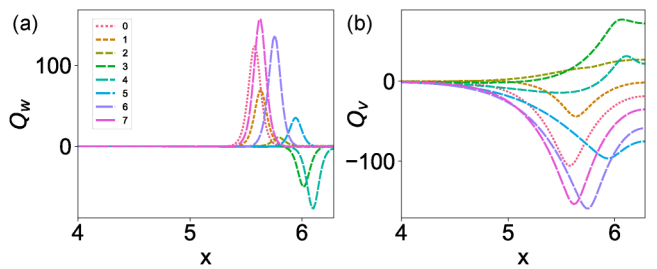

FIG. 2. (a) Phase sensitivity vector for w, shown in the domain $[4, L]$. (b) Same as (a), but for v.

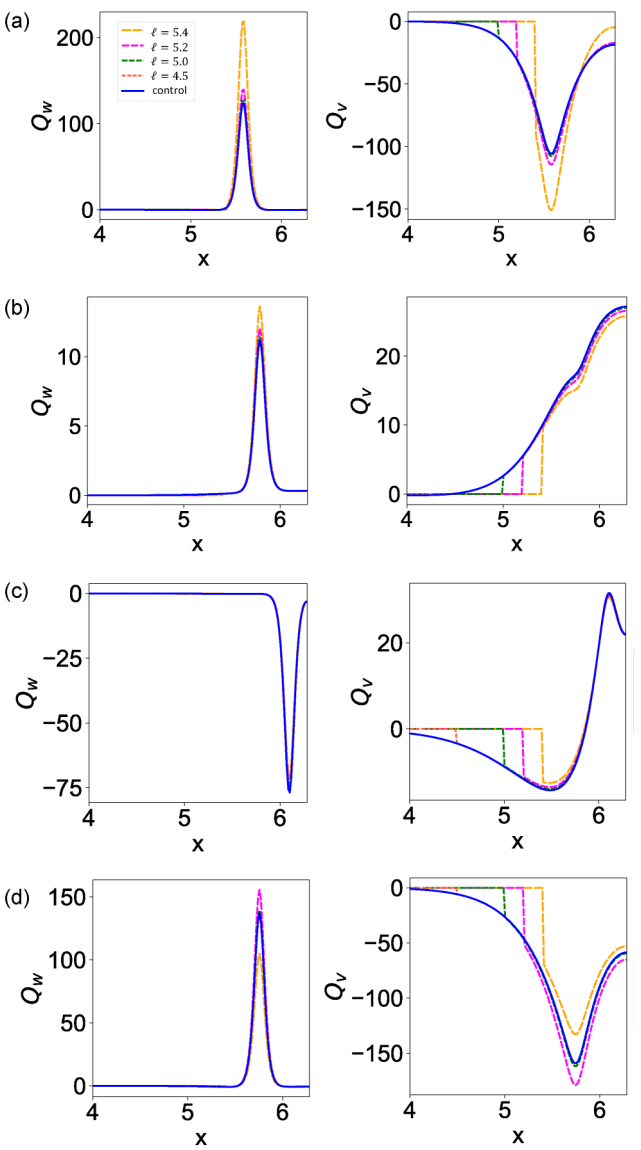

FIG. 3. Components of the phase sensitivity vectors, Q_w and Q_v. (a) Phase zero. (b) Phase 2. (c) Phase 4. (d) Phase 6.

approximately $1/k$ those of w and v. The w field shows a rapid change from positive to negative, which shows an interface.

Figure 1(b) shows the behavior of the breathing solution over one period by eight snapshots at equal time intervals. In this subsection, phase j corresponds to the time $t = jT/8$. The interface of w oscillated within a confined region $5.5 < x < L$. As shown in Fig. 1(b), the interface of w moved rightward in the former half of the period (phases from 0 to 4), and leftward in the latter half (phase during $4, \cdots, 7$ and 0), whereas the motion of v was slightly delayed; the distribution did not change the position significantly during the phases 0 and 1 as well as the phases 4 and 5. The shape of the v field during the right-moving interval differed from that of the left-moving interval, indicating that the interfaces did not maintain the shape owing to the nonlinear interaction between w and v.

The oscillation mechanism was explained in Ref. [20] as follows. The origin of the oscillation was due to the Hopf bifurcation from the steady solution, which occurs when τ is reduced. Therefore, even in the oscillation region, an unstable steady solution exists. Let us consider that the interface of w moves to the right (from the position of the interface of the unstable solution). Owing to the profile of w, w increased in the region where the interface was swept. The increase in w increased the value of v, owing to Eqs. (27) and (28). The increase in v reduced w owing to Eqs. (26) and (28). The reduction in w resulted in the interface moving in the inverse direction, and the interface of w was pushed to the left. Similar dynamics occurred when the interface moved to the left. These processes yielded the oscillations. However, it is noteworthy that the inhomogeneity of the periodic motion clearly shows that this periodic orbit in the phase space was far from a simple oscillation, and the phase response to perturbation is expected to exhibit a strong phase dependence.

2. *Projected phase sensitivity functions*

The phase sensitivity function was calculated using the method described in Ref. [11], and converted to the phase sensitivity vectors, Q_w and Q_v [11], which are shown in Fig. 2.

Figure 2 shows that Q_w assumed significant values in a region ($5 \leqslant x$) over one period. The peak of Q_w corresponded approximately to the position of the interface of w [Fig. 1(b)], although the magnitude and sign changed in one period. The values of Q_w were either positive (phases from 0 to 2 and 5 to 7) or negative (phases 3 and 4). Q_v was assumed in a relatively wider region ($4 \leqslant x$). The peak of Q_v also corresponded approximately to the position of the interface, and the values of Q_v were negative (phases from 0 and 1, and from 5 to 7) and positive (phase 2 and 3) or both (phase 4). These characteristics imply that the behavior near the LC was not symmetric under the translation $t \to t + T/2$, owing to the LC being far from the Hopf bifurcation point.

Next, we evaluate the phase sensitivity function using the projection method. Recall that the fields of w and v were discretized into a $2N$-dimensional space $W = \{w_1, \cdots, w_N, v_1, \cdots, v_N\} \in \mathbb{R}^{2N}$ where $w_j = w(j\Delta x, t)$, $v_j = v(j\Delta x, t)$, and $\Delta x = L/N$. We partitioned the computational domain $[0, 2\pi]$ into two regions, $[0, \ell)$(Region 1;R_1) and $[\ell, L]$(Region 2;R_2). Correspondingly, we defined two subspaces W_1 and W_2 as follows:

$$W_1 = \{w_j, v_j \mid j\Delta x \in R_1\}, \quad W_2 = \{w_j, v_j \mid j\Delta x \in R_2\}. \tag{29}$$

Subspaces W_1 and W_2 are characterized by the basis of W. If we define an orthonormal basis of W as $\{\boldsymbol{v}_1, \cdots \boldsymbol{v}_{2N}\}$ ($[\boldsymbol{v}_j]_i = \delta_{ij}$), the orthonormal basis of W_s ($s = 1, 2$) is $W_s = \mathrm{span}\{\boldsymbol{v}_j, \boldsymbol{v}_{N+j} \mid j = 1, \cdots, N,\ j\Delta x \in R_s\}$. In the following analysis, we use W_2 as the target region. The projection from W_2 to W defines the matrix V' in Sec. II C, by which the projection method can be applied.

The convergence of the inverse power method was determined based on the condition $|\boldsymbol{x}_k - \boldsymbol{x}_{k-1}| < 10^{-10}$ within 20 iterations. Figure 3(a) shows the phase sensitivity vectors in phase zero by the projection method. Here, the cases for $\ell = 0$ (control; blue solid curves) and $\ell = 4.5, 5.0, 5.2, 5.4$ are shown.

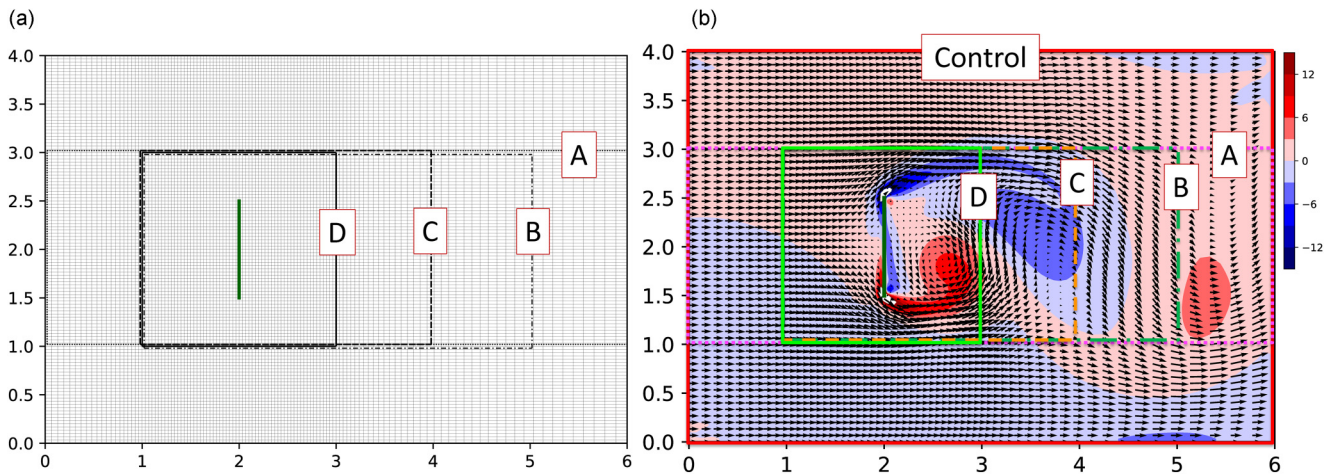

FIG. 4. (a) Computational grid and target regions. Target regions are displayed by rectangles with dotted lines A, dashed lines B, broken lines C, and solid lines D, respectively. Rectangles are slightly shifted such that each region can be clearly distinguished. (b) Velocity and vorticity fields. Target regions are shown as well.

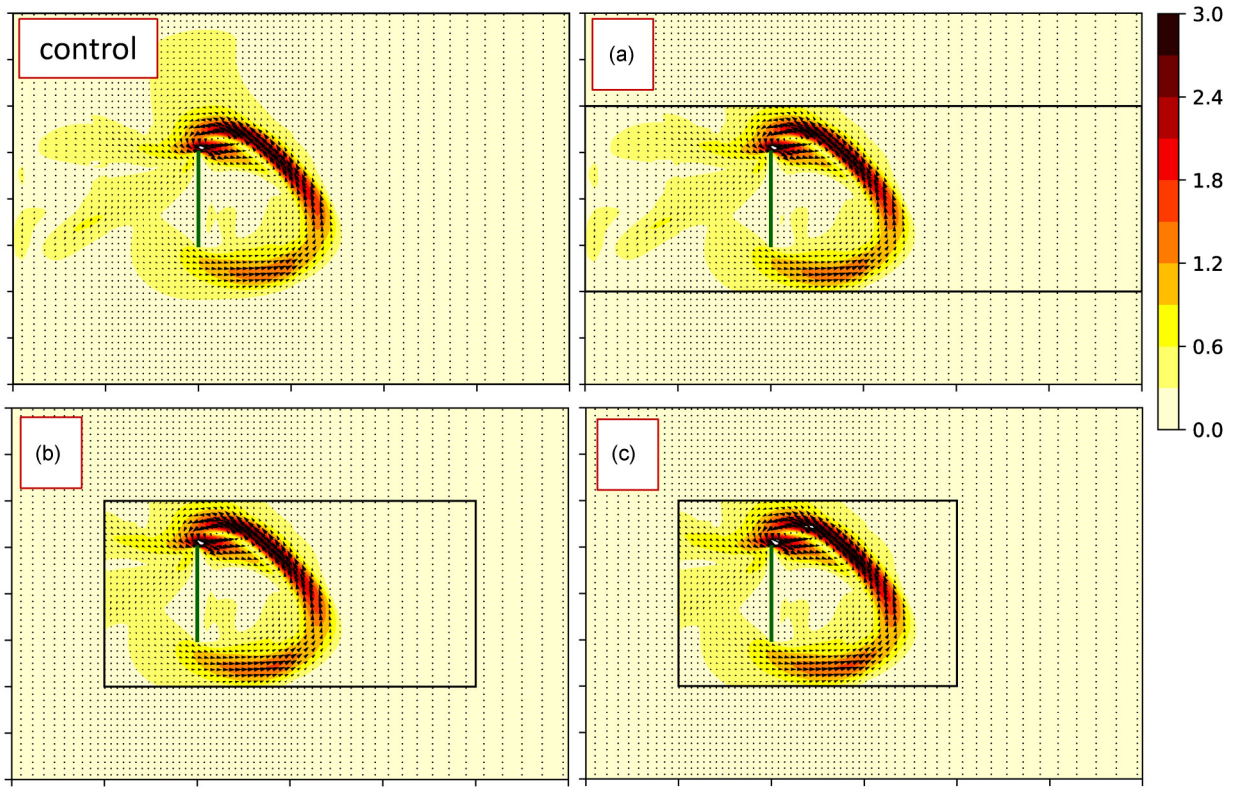

FIG. 5. Phase sensitivity vectors obtained using projection method. Colors indicate the magnitude of $|\boldsymbol{Q}|$. Regions A–C correspond to those shown in Fig. 4.

The validity of the target regions was evaluated using $\lambda_{\min}$, i.e., the absolute minimum Ritz values for the reduced equation (25). The values were $2.398 \times 10^{-4}(\ell = 4.5)$, $1.210 \times 10^{-2}(\ell = 5.0)$, $4.696 \times 10^{-2}(\ell = 5.2)$, $-1.606 \times 10^{-1}(\ell = 5.4)$, whereas 1.107×10^{-7} for the control case. When comparing with the profiles with the control case, we may conclude that the main profile can be restored when $\lambda_{\min}$ is approximately 0.1 or less, although the critical value depends on the accuracy demands. The ratio of the area (length) of R_2 to the entire region for the case where $l = 5.2$ is 17.2%.

Because of the change in variables, the orders of the magnitude of Q_w and Q_v were the same. Based on our selected values of ℓ, the major profile of Q_w was within the target region R_2 for all the cases presented, whereas a portion of the profile of Q_v was outside the target region when ℓ was large. We estimated the relative magnitude of the phase sensitivity function, ϵ_{b}, based on the absolute maximum Q_v in region R_1 to that in region R_2, i.e., 1.227×10^{-2} ($\ell = 4.5$), 0.1267 ($\ell = 5.0$), 0.2947 ($\ell = 5.2$), and 0.6521 ($\ell = 5.4$). The values of ϵ_{b} may correspond to ϵ in the analysis in Sec. II D.

In the cases where $\ell = 4.5$ and 5.0, the calculated Q_w and Q_v in the target region yielded almost the same profile as the control case. It is noteworthy that the target region was limited (28 and 20% of the entire region for $\ell = 4.5$ and 5.0, respectively). When $\ell = 5.2$, the profiles of Q_w and Q_v were consistent with the control case, although the absolute peak values of Q_w and Q_v were slightly larger than those of the control case. The case $\ell = 5.4$ provides an example of the resultant profiles if the target region does not encompass the major profiles. The profiles deviated from the control case, although the qualitative behavior was preserved. These results were consistent with the analysis in Sec. II D, where the error of the projected phase sensitivity function was $O(\epsilon^2)$ or less.

A similar analysis was performed for different phases (2, 4, and 6). The results, as shown in Figs. 3(b)–3(d), were consistent with the discussion for the case of phase zero.

B. Two-dimensional flow past a flat plate

We analyzed a two-dimensional viscous flow past a flat plate in a uniform flow. A fractional step method was used to solve the incompressible Navier-Stokes equations using an immersed boundary method [22]. The finite volume method was used for spatial discretization [23]. The Adams-Bashforth scheme and the Crank-Nicolson scheme were used for the time integration of the advection terms and that of the dissipation terms, respectively. The computational code was modified from that used in Ref. [11] except for the implementation of the immersed boundary method.

The domain size was $[0, 6c] \times [0, 4c]$, where $c(= 1)$ is the wing cord of the plate. For comparison, the domain size was set to be small such that the phase sensitivity function for the velocity in the entire region can be calculated within a reasonable time. A constant velocity was applied at the boundaries $x = 0$ and $y = 0, 4c$. The outflow boundary condition proposed by Dong *et al.* [24], which aims to minimize the domain truncation, was used for the boundary $x = 6c$.

The center of the plate wing was at $(x, y) = (2c, 2c)$ and the plate was perpendicular to the uniform flow direction. The

TABLE I. Ritz values for various target regions. "NA" indicates the cases where Ritz value did not converge under the prescribed conditions.

Target region	Ritz value	Symbol
$[c, 3c] \times [c, 3c]$	NA	D
$[c, 4c] \times [c, 3c]$	-1.07×10^{-1}	C
$[c, 5c] \times [c, 3c]$	-8.20×10^{-2}	B
$[c, 6c] \times [c, 3c]$	-5.55×10^{-2}	
$[0, 6c] \times [c, 3c]$	-5.25×10^{-2}	A
$[0, 6c] \times [0.5c, 3.5c]$	5.05×10^{-3}	
$[0, 6c] \times [0, 4c]$	7.36×10^{-3}	Control

uniform flow velocity was $(U, 0)$ $(U = 1)$ and the Reynolds number was $\mathrm{Re} = Uc/\nu = 200$, where ν is the kinematic viscosity. An unequal and orthonormal grid was used, although the grid spacing in the region around the plate wing was uniform, $c/30$. The number of grid points was 120×120 [Fig. 4(a)].

The periodic solution was obtained numerically using the Newton-Raphson method [15] under the condition where the relative errors of both the residue and the increment of the iteration were less than 10^{-11}. The period was $T = 4.042\,64$ when a single period was segmented into $1408 = 2^7 \times 11$ time steps. The origin of the phase was set at the time when the maximum lift was attained.

The projection method was used to obtain the projected phase sensitivity function for the target regions described below. In this calculation, we focused on the response to the perturbation to velocity components, $\boldsymbol{u} = (u, v)$ alone, whereas the response to the pressure and previous time step was not calculated, contrary to the description in Sec. III A, where the entire degree of freedom was used to obtain the phase sensitivity function. The convergence condition for the inverse power method was the same as that detailed in Sec. III A 1, and the Ritz value was labeled as nonavailable (NA) if the condition was not satisfied.

Figure 4(b) shows a snapshot of the vorticity field at phase zero. Five target regions were selected: (Control) $[0, 6c] \times [0, 4c]$, (A) $[0, 6c] \times [c, 3c]$, (B) $[c, 5c] \times [c, 3c]$, (C) $[c, 4c] \times [c, 3c]$, and (D) $[c, 3c] \times [c, 3c]$. These regions were related to the distribution of the coherent vortices; two coherent vortices with a positive sign and one coherent vortex with a negative sign are shown in Fig. 4. The target region can be characterized by the subspace of the space determined

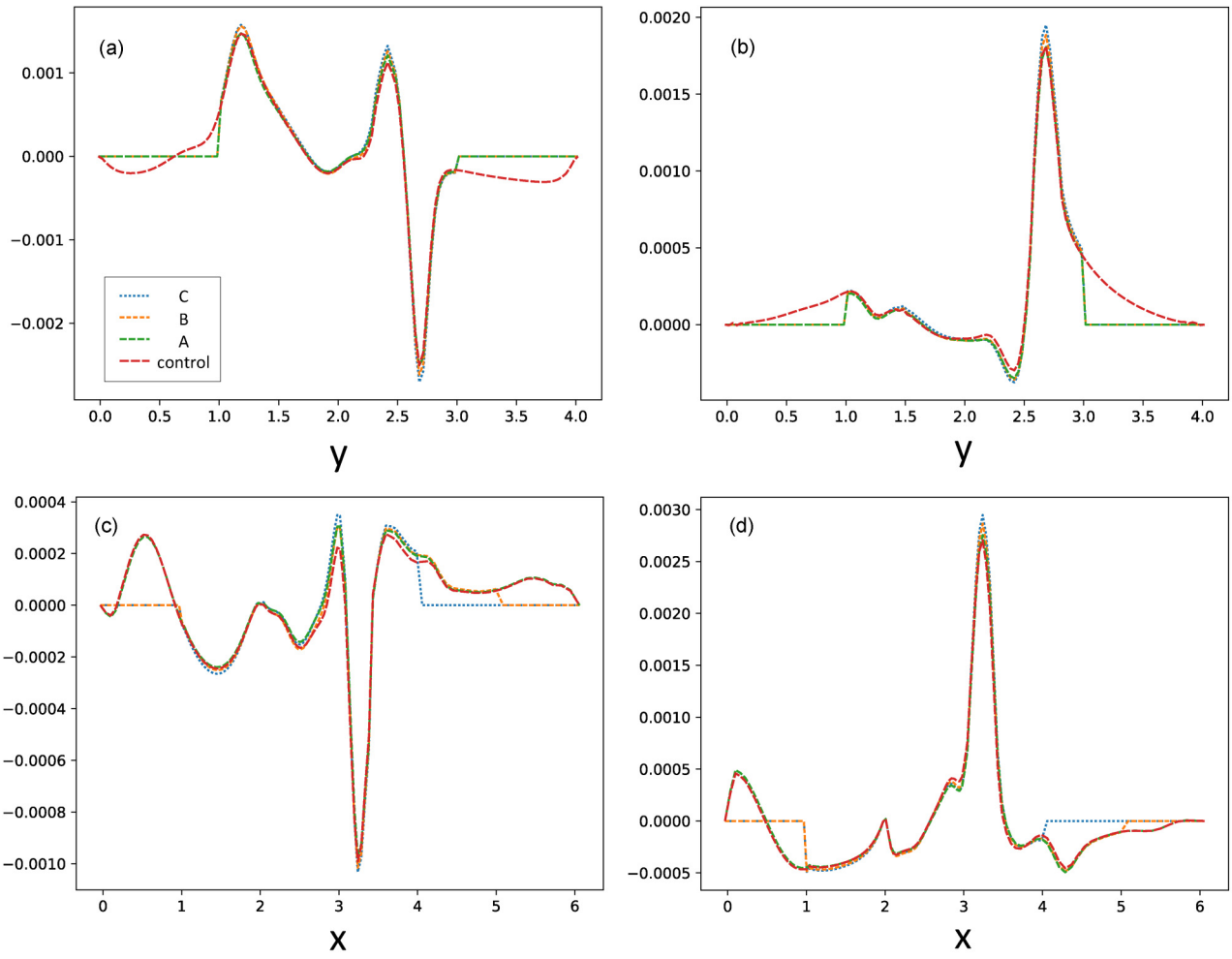

FIG. 6. Distributions of phase sensitivity functions obtained using the projection method along cross lines. (a) $\tilde{Z}_w$ along line $x = x_c(= 2.5)$. (b) $\tilde{Z}_v$ along line $x = x_c$. (c) $\tilde{Z}_w$ along line $y = y_c(= 2.0)$. (d) $\tilde{Z}_v$ along line $y = y_c$.

by the discretized computational domain in a similar way described in Sec. III A. Figure 5 shows the phase sensitivity vector [11], $\boldsymbol{Q} = (Q_u, Q_v)$. We remark that the phase shift due to the perturbation $\Delta \boldsymbol{u}\, \delta(\boldsymbol{x} - \boldsymbol{x}_0)$, where $\Delta \boldsymbol{u}$ and $\delta(\boldsymbol{x})$ represent a constant perturbation vector and the three-dimensional delta function, respectively, is expressed as $\Delta \boldsymbol{u} \cdot \boldsymbol{Q}(\boldsymbol{x}_0)$ [11]. The Q field obtained using the projection method for the regions A, B, and C was almost the same as that of the control field, whereas the field of $|\boldsymbol{Q}|$ assumed values outside and above the region A in the control case (Fig. 5, "control"). The comparison suggests that the proposed method works well even if the target region is small.

To compare these fields in detail, we present the functions $\tilde{Z}_u(0)$ and $\tilde{Z}_v(0)$ along the lines $y = y_c(= 2.0)$ and $x = x_c(= 2.0)$ in Fig. 6. Even in the region C, the functions agreed well with those for the case with the control region, although the values of the functions $\tilde{Z}_u(0)$ and $\tilde{Z}_v(0)$ outside the region C were not negligible. Such characteristics of the projection method corresponded well to the results provided in Sec. III A.

For a quantitative assessment, the Ritz values for various target regions, including regions A–D and the control case, are listed in Table I. For region D, the inverse power method did not converge under the prescribed iteration condition ("NA" in the table), implying that the absolute Ritz value was not sufficiently small. A comparison between the control field and the Q field (Fig. 5), as well as the cross-section fields (Fig. 6), suggests that the target regions in which the Ritz value was approximately 0.1 or less yielded a reasonable Q field, although dependency on the required accuracy was involved.

IV. CONCLUDING REMARKS

Herein, we have proposed a method to calculate the phase sensitivity function in a target domain that can be used in conjunction with the Jacobian-free method to obtain the phase sensitivity function using only the time evolution of the system [11].

The proposed method utilizes the Rayleigh-Ritz procedure, which approximates the eigenvalues and the eigenvectors for a large system by considering an appropriate subspace. Combined with the inverse iteration method, this method provides an approximation of the phase sensitivity function as the eigenvector of the zero (absolute minimum) eigenvalue.

This method was demonstrated via an analysis of the breathing solution of a reaction-diffusion system, in which an interface oscillated in a confined region and no significant change occurred in the other wide region. It was demonstrated that the proposed method functioned as intended; the phase sensitivity function in the target region was similar to the original one, even when the relative area (length) of the target region was less than 20% and the computational time was reduced significantly. The error depended on the width of the region in which the major part of the phase sensitivity function was contained.

In addition, we analyzed the flow past a flat plate to analyze the dependency of the phase sensitivity functions on the area of the target region. Although we omitted the response to the pressure and information from the previous time step, we successfully obtained the approximation of the phase sensitivity functions, although an extremely small target region did not provide good results. The analysis of this case suggested that even the omission of a variable and the spatial region enabled the estimation of the phase sensitivity function.

The projection method can be used in a more complicated system; its application to two-dimensional or three-dimensional PDE problems with different time scales will significantly reduce the computational cost. This will be investigated in future studies.

ACKNOWLEDGMENTS

This work was partially supported by Japan Society for the Promotion of Science KAKENHI Grant No. 19K03671 and SECOM Science and Research Foundation.

[1] Y. Kuramoto, *Chemical Oscillations, Waves, and Turbulence* (Dover, New York, 1984).
[2] H. Nakao, Contemp. Phys. **57**, 188 (2015).
[3] B. Ermentrout, Neural Comput. **8**, 979 (1996).
[4] K. Taira and H. Nakao, J. Fluid Mech. **846**, R2 (2018).
[5] M. A. Khodkar and K. Taira, J. Fluid Mech. **904**, R1 (2020).
[6] M. A. Khodkar, J. T. Klamo, and K. Taira, Phys. Rev. Fluids **6**, 034401 (2021).
[7] I. A. Loe, H. Nakao, Y. Jimbo, and K. Kotani, J. Fluid Mech. **911**, R2 (2021).
[8] Y. Kawamura and R. Tsubaki, Phys. Rev. E **97**, 022212 (2018).
[9] Y. Kawamura, Phys. Rev. Res. **1**, 033130 (2019).
[10] J. P. Keener, *Principles of Applied Mathematics: Transformation and Approximation* (CRC Press, 2018).
[11] M. Iima, Phys. Rev. E **99**, 062203 (2019).
[12] C. H. K. Williamson, Annu. Rev. Fluid Mech. **28**, 477 (1996).
[13] M. Iima, in *Proceedings of NOLTA 2019*, 2019 (unpublished).
[14] V. Novičenko and K. Pyragas, Nonlinear Dyn. **67**, 517 (2011).
[15] Y. Saiki, Nonlinear Processes Geophys. **14**, 615 (2007).
[16] L. D. Landau and E. M. Lifshitz, *Fluid Mechanics*, 2nd ed., Course of Theoretical Physics Vol. 6 (Butterworth-Heinemann, Washington, DC, 1987).
[17] Y. Saad, *Numerical Methods for Large Eigenvalue Problems*, Revised ed. (SIAM, Philadelphia, 2011).
[18] T. Ikeda and Y. Nishiura, SIAM J. Appl. Math. **54**, 195 (1994).
[19] Y. Nishiura and M. Mimura, SIAM J. Appl. Math. **49**, 481 (1989).
[20] T. Ohta, A. Ito, and A. Tetsuka, Phys. Rev. A **42**, 3225 (1990).
[21] Y. Nishiura, *Far-From-Equilibrium Dynamics* (American Mathematical Society, Providence, 2002).
[22] M. Uhlmann, J. Comput. Phys. **209**, 448 (2005).
[23] H. Liu and K. Kawachi, J. Comput. Phys. **146**, 124 (1998).
[24] S. Dong, G. Karniadakis, and C. Chryssostomidis, J. Comput. Phys. **261**, 83 (2014).